*Regular Article*

# Heart Rate Variability Monitoring under Stimulation Input Using Non-Contact CW Radar

**Hoang Thi Yen[1], Van-Phuc Hoang[1], Guanghao Sun[2]**

[1] Le Quy Don Technical University, Hanoi, Vietnam
[2] The University of Electro-Communications, Tokyo, Japan

Correspondence: Hoang Thi Yen, yenht@lqdtu.edu.vn
Communication: received 24 March 2024, revised 07 May 2024, accepted 12 May 2024
Online publication: 03 July 2024, Digital Object Identifier: 10.21553/rev-jec.370

*Abstract*– **Recent studies have mainly relied on radar technology for extracting crucial vital signs because of its ability to measure without physical contact. The focus on deriving cardiac interbeat interval and heart rate variability has gained significance due to its complexity and relevance in healthcare. Our investigation involved a detailed analysis of continuous wave radar signals to enhance the extraction of chest wall movement data. Using a convolution algorithm, we eliminated the respiratory component from the signal, while a locally projective noise reduction algorithm helped isolate the heartbeat component. Subsequently, a derivation filter was applied to pinpoint the R peak of the heartbeat, facilitating the collection of IBI and HRV metrics. This methodology proved effective for individuals in a relaxed, motionless state. However, its efficacy in cases of elevated heart rates caused by factors such as exercise or caffeine consumption remained uncertain. For subjects with large changes in heart rate followed by large changes in cardiac IBI, we made a small improvement in the algorithm. By performing a window shift of 10 seconds with an overlap of 1 second. Each 10-second data segment is fed into the algorithm. At each data segment, we perform multiple iterations with decreasing number of neighbors until no further change is made. With this adjustment, the results achieved in the group of subjects using input stimulation to increase heart rate such as exercise, or drinking coffee were indicated a strong correlation of 96.38% between radar-based measurements and reference measurements for this group of subjects, affirming the effectiveness of the proposed method in such scenarios.**

*Keywords*– **Non-contact, 24 GHz CW radar, vital sign, cardiac IBI, HRV.**

## 1 Introduction

The prioritization of health remains a perennial focal point of significant importance, in which a person's physical condition is assessed through vital signs [1, 2]. Even in the hospital, patients are also monitored for these indicators through measuring devices. Key vital signs include body temperature (BT), blood pressure (BP), respiratory rate (RR), heart rate (HR), and heart rate variability (HRV). There are two methods of measuring vital signs based on the measurement principle: contact and non-contact methods. Contact measurement includes traditional techniques in which medical devices are placed on the skin to record specific parameters. Through a conversion process within the device, these devices provide vital signs readings. Non-contact method is the measurement of vital signs at a fixed distance from the individual being assessed. Currently, contactless devices are promised for sustainable development thanks to their benefits such as no physical contact, comfortable to use, suitable for long-term monitoring, especially in the context of epidemic. Various non-contact methods are used to obtain vital signs by processing images and videos recorded from cameras [3–7]. Some studies utilize radar technology as monitor of vital signs [8–16]. Additionally, Ballisto-cardiography (BCG) records the body movements caused by the heart's ballistic forces-the contractions and ejection activities-which are then amplified and recorded on motion chart paper later when the receiver converts it into an electrical signal. BCG facilitates the monitoring of cardiac and respiratory activity, typically by focusing on an external pressure or strain gauge to detect vibrations from the mechanical activity of the heart and lungs [17–19]. The RGB camera detects changes in blood flow by capturing light in red, green, and blue wavelengths (RGB) in facial blood vessels to gauge heart rate, leveraging the specific responsiveness of facial skin to these changes. This method entails capturing a concise video with numerous frames and subsequently using algorithms to assess the colour properties of pixels across these frames, thereby determining the heart rate [6, 7]. Infrared cameras are utilized to measure both respiration and body temperature. Exhaled air, originating from the lungs, raises the temperature in the nasal area, while inhaled air is from the mouth, lowers the temperature in this region. Through detecting temperature shifts in the nasal area, the infrared camera identifies these fluctuations, representing the respiratory rate [7].

Radar technology is employed for measuring RR, BP, HR and HRV. It tracks movements on the body surface caused by respiratory and cardiac rhythms, extracting information regarding these pivotal indicators [13–16]. Radar-based blood pressure measurement involves detecting phase changes at two points on the body. Deter-

mining the interval between the highest phase values aids in predicting systolic and diastolic blood pressure values using specific algorithms [20, 21]. HRV reflects variations in the time intervals between heartbeats, known as cardiac inter-beat intervals (IBI), influenced by the autonomic nervous system [22, 23]. A healthy heart does not beat rhythmically as a metronome; rather, it exhibits continuous variations measured in milliseconds between beats. HRV serves as a quantifiable reflection of the balance between the sympathetic and parasympathetic influences and has been utilized as an indicator of cardiovascular health and a predictive factor for cardiovascular outcomes. Detecting IBI within cardiac signals to extract HRV features holds immense significance in the medical field [24]. The low frequency (LF) power of HRV during controlled respiration stands as a robust indicator for sudden death among chronic heart failure patients [25]. This involves deriving various time and frequency-based parameters from recordings. For instance, a mere 2-minute ECG recording can predict hospitalization due to end-stage renal disease and chronic kidney disease in participants of studies called the Atherosclerosis Risk in Communities [26].

In our previous paper [23], we implemented an effective method to estimate and detect non-contact HRV using radar, employing in time-frequency domain. This article builds upon the research [23], presenting a comparative analysis of our method's effectiveness against other studies. Additionally, this study examines radar's capacity to track IBI and HRV in a group subjected to stimuli that increase heart rate, exploring the feasibility of 24 GHz continuous wave (CW) radar in monitoring HRV not just during rest but also during situations with increased heart rate risks. During the experiment, three volunteers engaged in vigorous exercise, such as rapid jumping, and one volunteer consuming coffee to induce a higher-than-normal heart rate. Throughout the exercise, all three volunteers experienced an increase in heart rate to around 100 beats per minute, and their signals were recorded using both ECG and 24 GHz CW radar. For vital sign measurement by radar, the frequency domain comprises the main peak and its harmonics because the distorted signal exhibits periodicity at the same frequency as the fundamental component of breath. Subsequently, the estimation of heart rate in the presence of the third harmonic is a challenging topic in frequency domain analysis. To address this, our proposed method integrates both frequency and time-domain analyses to achieve precise IBI estimation. Parameters are selected through frequency domain analysis and applied in the time domain, where peak decision-making occurs. This approach proves effective when the heartbeat frequency closely corresponds with the third-order harmonic of breath.

This work makes significant contributions as the following:

1. Describes the research method to estimate and detect non-contact HRV using radar.

2. Presents a comparative analysis of proposed method's effectiveness against other studies.

3. Improve the algorithm to track IBI and HRV in a group subjected to stimuli that increase heart rate by performing multiple iterations with decreasing number of neighbors until no further change is made.

The remainder of the article is arranged as follows. Section II briefly describes the research method for cardiac IBI detection and the HRV analysis method including fast Fourier transform (FFT) and autoregressive (AR). Section III presents results compared with other studies of the same purpose of finding IBI and HRV. The results of IBI and HRV analysis on three volunteers under the influence of stimulation are presented in section IV. Section V gives discussion and conclusion.

## 2 Research Method

### 2.1 Radar and Ability to Capture Vital Sign

This section will present the structure of radar and the ability to track vital sign signals. The structure of the Doppler 24 GHz CW radar (New Japan Radio, NJR4262) is shown in Figure 1. It can be considered that the oscillator creates a sine wave, this wave is transmitted to hit the wall of the human body, the reflected wave returns also in the form of a sine wave with the signal phase changing. The changes due to the Doppler effect with chest wall movement. In the radar structure, there is a multiplier, this multiplier multiplies the transmitted signal and the received signal, then the filter filters out the high-frequency signal to obtain the I and Q channel signals. These signals carry information about the movement of the chest wall.

Information about the movement of the body wall due to breathing and heart rate is contained in the phase of the signal channel. Based on the I channel and Q channel signals, we can detect the displacement of the measured object. The signals of I channel and Q channel carry information about the movement towards the radar and movement away from the radar of the measuring object. The chest wall goes approaching the radar when the person inhales, because the chest is filled with air then moves closer to the radar. And vice versa, the chest wall goes leaving the radar when the person exhales, the lungs release exhaled air then moves away from the radar. While breathing, the heart beating also makes the chest move closer and farther away from the radar with a frequency 3 to 4 times greater than the breathing frequency.

The changing in phases of the I and Q output vary based on the direction of the target's movement, illustrated in Figure 2. When the chest wall is approaching, the Q output experiences a 90-degree delay from the I output. Conversely, when the target is leaving, the Q signal is 90 degrees ahead of the I signal. This phase difference during approaching and leaving enables radar to detect the movement of the chest wall. By arranging the device appropriately, the radar can detect the chest's motion towards or away from it during inhalation and exhalation. Monitoring the phase shift in the I and Q channels enables the observation of chest

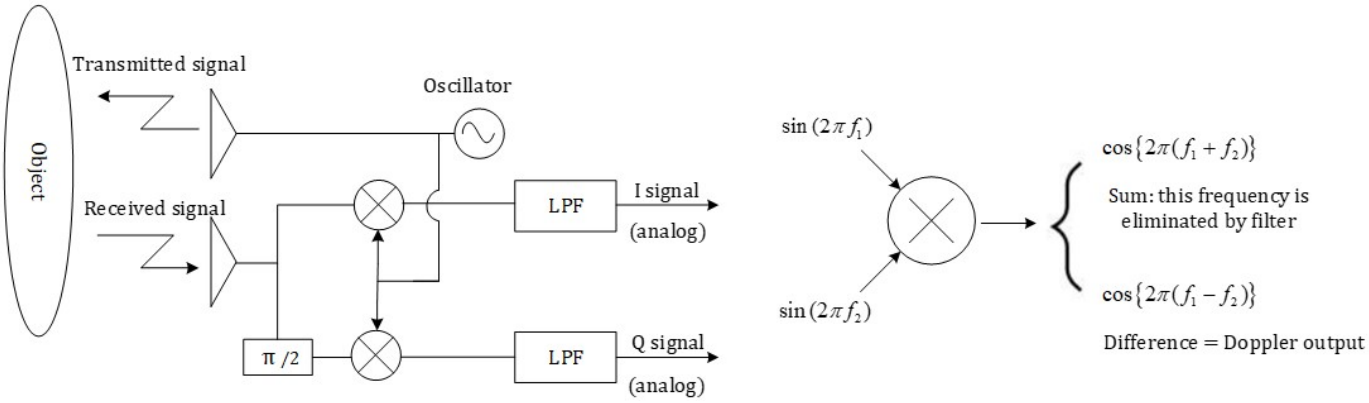


Figure 1. The structure of CW Doppler radar.

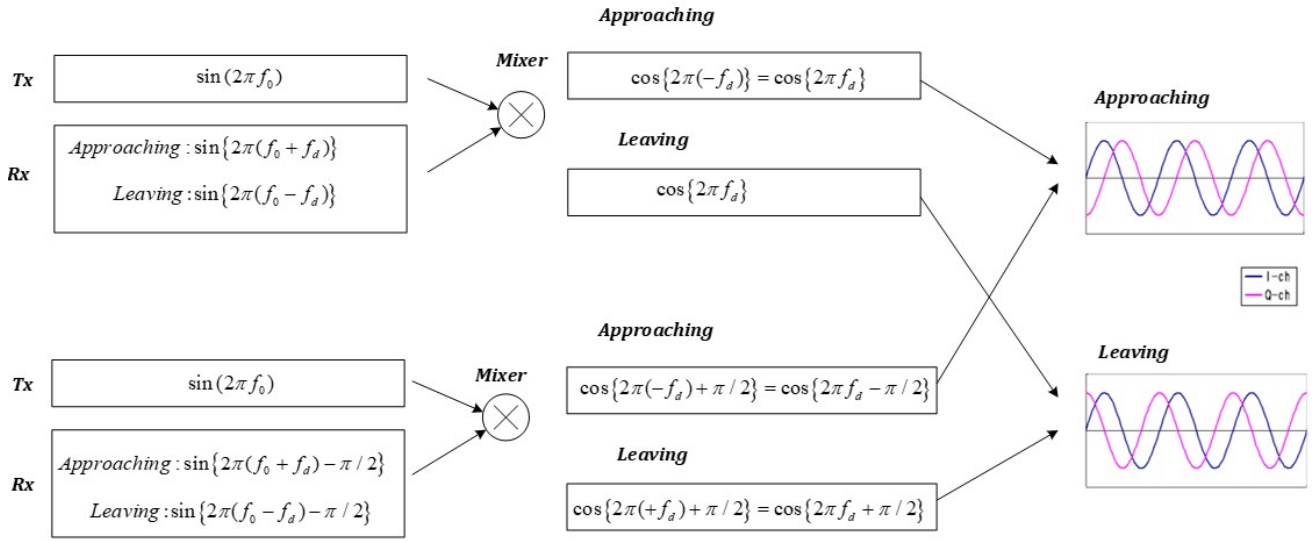


Figure 2. Doppler radar principle for extracting base-band signal.

wall movements during breathing and even the surface-level heartbeat in the chest area.

### 2.2 Proposed Method of Time-Frequency Domain

For the movements longer than half the radar wavelength (the half wavelength of a 24 GHz radar is approximately 6.2 mm), it is required to use both I and Q signal channels to extract information about the measured object's movement. However, for movements smaller than half a wavelength, using a signal channel provides simplicity and efficiency as investigated in [27]. In this study, the signal processing algorithm is performed on one radar signal channel after performing signal evaluation and selecting one channel as below. Radar is placed under the bed to sense the movement of the chest surface due to the vital sign. The received radar signal includes two signal channels: I channel and Q channel. A signal channel selection block will select one channel with a larger standard deviation to send to the next processing. First the breathing rate component is estimated using a convolutional filter. This component is subtracted from the signal. Next, the heartbeat component was estimated using the locally projective noise reduction (LPNR) technique. LPNR operates by estimating the noise-free time series' structure in the delay embedding space using a local linear approximation [28]. Then a derivation filter is performed to clarify the R peak on the signal amplitude background. When peak R is found, cardiac IBI and HRV are obtained. A block diagram of the proposed method is shown in Figure 3.

In the proposed method, when utilizing the convolution filter, if *Tconv* exceeds the average of one beat time ($60 * f_{HR}$), the resulting smoothed signal will encompass both the heart component and noise. Consequently, subtracting to isolate the combination of HR information and noise leads to loss of heartbeat information. Conversely, if *Tconv* is smaller than the average of one beat time ($60 * f_{HR}$), the subtracted signal will retain information about respiration as well. Thus, calculating *Tconv* based on an average heart rate cycle yields optimal performance, and the smoothing technique is employed to isolate the respiration component. In addition, LPNR functions by approximating the manifold of the noise-free time series within the delay embedding space via local linear estimation. It subsequently maps the noisy measured delay vector onto this identified manifold [17]. In this context, delay embedding entails reconstructing a state-space representation from an observed one-dimensional time se-

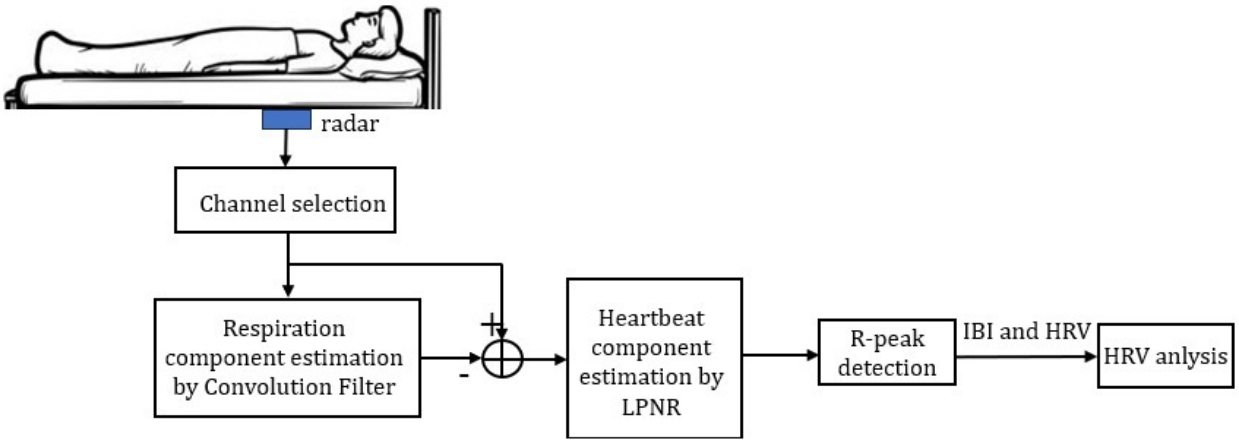


Figure 3. Diagram of proposed method for IBI and HRV detection.

ries, accomplished by forming delay vectors consisting of a specified number of consecutive samples from the time series.

### 2.3 HRV Analysis and HRV Features

Frequency domain analysis involves examining signal levels within specific frequency bands. In the context of heart rate variability, certain frequency ranges correspond to different physiological processes, such as activity in the parasympathetic nervous system. Techniques of FFT and AR methods are utilized to convert time-based data into frequency-based data. The FFT algorithm is relatively straightforward and computationally efficient. However, FFT-based spectral analysis faces challenges of non-uniform RR intervals and the need for stationary data segments. The length of these segments impacts the fundamental oscillation and frequency resolution in FFT analysis. FFT-based HRV analysis requires at least a stable 5-minute ECG segment, this limits its application. On the other hand, AR-based spectral analysis does not necessitate interpolation and requires shorter data lengths. However, the difficulty of AR method lies in its complexity due to varying model choices and orders across different studies [24]. In this study, the covariance method with an order of 16 was employed.

Respiration induces noticeable changes in heart rate, known as respiratory sinus arrhythmia (RSA). During inhalation, decreased intrathoracic pressure leads to reduced vagus nerve stimulation, increasing heart rate. Conversely, during exhalation, increased intrathoracic pressure activates baroreceptors and vagus nerve stimulation, reducing heart rate. The respiratory sinus arrhythmia component is typically observed as a high-frequency component (HF: 0.15-0.4 Hz), when the respiratory rate is within the HF band. The HF (or RSA) component of HRV is caused by parasympathetic regulation and thereby reflects parasympathetic nervous system activity. Another conspicuous component of HRV is the low frequency component (LF: 0.04-0.15 Hz) which is associated with baroreflex, where both sympathetic and parasympathetic activities influence LF oscillations, with dominance by the sympathetic nervous system.

In this study, after transforming the time series IBI data into frequency data, we discuss HRV features in the common frequency domain including: HF power is the power in the range of 0.15-0.40 Hz. LF power is between 0.04-0.15 Hz. LF/HF is the ratio between low frequency and high frequency power, reflecting the balance of the autonomic nervous system. The power of high-frequency component indicates the influence of parasympathetic regulation on heart rate, showing a notable decrease in sympathetic activity towards the sinus node above 0.15 Hz. On the other hand, the intensity of signals in the low-frequency (LF) range represents a combination of both sympathetic and parasympathetic activation [29]. To obtain accurate lower frequency measurements, it requires longer reading times, with minimum of 4 minutes. Actual activity in that frequency range is often expressed in terms of power, using units of milliseconds squared for a particular Hertz range. This means that the energy is calculated by the area under the curve. According to previous studies, the minimum reading time should be 2 minutes for reliability of low frequency (LF) power values. High frequency (HF) power can be reliably measured for 60 seconds. In our research, we measured 18 subjects for at least 2 minutes [23]. In this paper, three measurement subjects were taken for 5 minutes to ensure the accuracy of HRV observations.

## 3 Results of Comparison

In this section, we would like to make some comparisons with previous studies as the following. Study [30] introduces a method aimed at monitoring HRV using frequency-modulated continuous-wave (FMCW) radar. The process involves separating echo signals from different distances and improving signal quality by applying beamforming techniques. Following this, the phase indicating chest wall movement is demodulated, allowing for the calculation of acceleration to enhance heart rate and reduce respiration-related impacts. The refined acceleration pattern aids in estimating time intervals between heartbeats. Finally, the study devises a cooper-

Table I
Some Comparison to Study [30] Based on Time-Domain Features

| Comparison points | Research [30] | Our research |
|---|---|---|
| Type of radar | FMCW | CW |
| Number of subjects | 10 | 18 |
| Correlation coefficient of scatterplot | 0.9747 | 0.9743 |
| SDNN (ms) error | 3.5 | 1.2 |
| RMSSD (ms) error | 6.55 | 3.7 |
| MEAN (ms) error | 0.9 | 0.2 |
| RMSE | 14.9 | 16.51 |

ative optimization algorithm to precisely divide the acceleration signal, enabling a comprehensive HRV analysis. Some comparison points based on time-domain features are listed on Table I. In Table I, the root mean square error (RMSE) is a closely associated and commonly employed metric for assessing the disparities between HRV obtained from ECG and HRV values estimated via radar. Standard deviation of IBIs (SDNN) computes the mean HRV values in milliseconds and indicates the deviation of HRV from that mean at any given moment. Widely regarded as the benchmark for medical risk assessment, SDNN is instrumental in categorizing cardiac risk levels. Its values are predictive of both illness and mortality outcomes. The root mean square of successive differences (RMSSD) serves as a widely-used statistical gauge of HRV. It calculates the time intervals between consecutive heartbeats in real-time, providing an immediate RMSSD score. This approach proves beneficial in scrutinizing the effects of training intensity and recovery phases. Such statistical analysis enables the extraction of meaningful health insights from extensive data collections. It can be seen that our study achieves better results when errors occur in SDNN, RMSSD and MEAN are lower, while correlation coefficient of scatterplot is almost the same and RMSE is higher than in study [30].

Research [16] estimated HRV parameter using impulse-radio Ultra-wideband (IR-UWB) radar measured from the front of body. The authors did not analyze the parameter of IBI in time domain but parameter of HRV in three stages of rest and fatigue. Thus, to make a fair comparison, we will compare our results with the results of the resting period in [16]. The comparison can be shown as Table II. In which, lower standard mean deviation (SMD) values suggest that the HRV indices are tightly grouped around the mean, indicating higher reliability. Our research demonstrated a lower SMD compared to the study referenced as [16]. The calculation of SMD involves taking the square root s of the average variance in the denominator, in which $s_1^2$ and $s_2^2$ refer to the variance of values obtained by radar and ECG.

$$s = \sqrt{\frac{s_1^2 + s_2^2}{2}} \tag{1}$$

The SMD (Cohen's SMD) is then calculated as equation (2), where $\overline{x_1}$ and $\overline{x_2}$ indicate the averages of cardiac IBI values obtained from radar and ECG respectively.

$$SMD = \frac{\overline{x_1} - \overline{x_2}}{s} \tag{2}$$

This study offers several benefits in terms of the practical setup within hospital systems. Specifically, the type of radar used is CW radar which is known for its low power consumption and straightforward design. Placing the radar beneath the bed also alleviates the mental strain on patients. In addition, study [31] used UWB radar with center frequency of 79 GHz, sampling rate at 500 Hz, bandwidth of 2 GHz, evaluated IBI of three healthy subjects. The authors used 2 radars, measured the motion of chest and shoulder with 5 min per subject. The result of average error RMSE was 26.7 ms which is bigger than that of our study with 16.51 ms. Lastly, we could give some comparison with results using the same type of CW Doppler radar as Table III. The proposed method tested on a larger group of indivisuals, showed an improved accuracy with an average RMSE of 16.51 ms and an average MRE of 1.22%. The lower values for RMSE, MRE, and SMD indicate better results. Lower MSD values signify that the HRV indices were more tightly clustered around the mean, indicating higher reliability.

## 4 Results on Subjects with Stimulation Input

For subjects with large changes in heart rate followed by large changes in cardiac IBI, we made a small improvement in the algorithm. By performing a window shift of 10 seconds with an overlap of 1 second. Each 10-second data segment is fed into the algorithm. At each data segment, we perform multiple iterations with decreasing number of neighbors until no further change is made. With this adjustment, the results were achieved in the group of subjects using input stimulation to increase heart rate such as exercise, or drinking coffee as shown below. This study was approved by the Ethics Committee of the University of Electro-Communications under application number No. 16031. All members gave their consent in written form after being informed.

The Figure 4 displays the original signal captured by radar and ECG for three individuals including: a) A 33-year-old female, weighing 58 kg, standing at 1.61 m with a resting heart rate ranging between 55-65 beats per minute (bpm); b) A 34-year-old male, weighing 68 kg, standing at 1.69 m with a resting heart rate ranging between 75-80 bpm; and c) A 26-year-old male,

Table II
Some Comparison to Study [16]

| Comparison points | Study [16] | Our study |
|---|---|---|
| Type of radar | IR-UWB | CW Doppler |
| Centre frequency | 8.7 GHz | 24 GHz |
| Bandwidth | 1.5 GHz | - |
| Number of subjects | 15 | 18 |
| Measured time per subject (min) | 8 | 2 |
| Sampling rate | 250 Hz | 1000 Hz |
| SMD for LF | 0.771 | -0.021 |
| SMD for HF | 0.739 | 0.016 |
| Measured on healthy subjects | Front | Back |

Table III
Some Comparison to [13] and [14] using the same type of CW Doppler Radar

| Research | Radar Frequency (GHz) | Number of subjects | Measured time per subject (s) | Average RMSE (ms) | Average MRE (%) | SMD of LF | SMD of HF |
|---|---|---|---|---|---|---|---|
| [13] | 24 | 10 | 120 | 47.5 | - | - | - |
| [14] | 24 | 10 | 180 | 16.7 | 1.54 | -0.167 | 0.018 |
| Proposed method | 24 | 18 | 120 | 16.51 | 1.22 | -0.021 | 0.016 |

weighing 71 kg, standing at 1.72 m with a resting heart rate ranging between 80-90 bpm. Subject a and b were measured after exercising, while subject c exercised and consumed coffee before measurement of 5 minutes. The figures on the left represent the raw signal obtained from the device, above is the drawing of the radar signal. It is very interesting that the amplitude of the radar signal gradually decreases as breathing becomes more relaxed. The results on the right show that the proposed method using radar can track cardiac IBI. Subjects measured after vigorous exercise had cardiac IBI less than 600 ms, meaning the heart rate was greater than 100 bpm. After that, cardiac IBI gradually increased and stabilized at the average level of subjects.

Researchers have noted that a significant increase in sympathetic nervous system activity and decreased parasympathetic input immediately after vigorous exercise (indicating low HRV post-exercise) may resemble patterns observed during a cardiac event [32, 33]. The limited sample size prevents drawing statistical conclusions from the measured individuals. However, the simulation outcomes and interviews with the three volunteer members largely align with prior statistical findings derived from contact sensors [34]. In Figure 4a, the depicted individual, who maintains a regular exercise routine, exhibits consistently low heart rates. Radar signals indicate rapid decreases in breathing amplitude, coupled with swift recovery, suggesting rapid recovery of bodily equilibrium. Calculations reveal a quick recovery of HRV from approximately 600 ms to over 1000 ms, with significant fluctuations of around 300 ms, consistent with active individuals. Conversely, the individual shown in Figure 4b, as per interviews, infrequently exercises and occasionally consumes alcohol. Radar measurement shows a decrease in breathing amplitude with body condition recovery. However, HRV recovery is less substantial, increasing from 625 ms to 800 ms, with modest fluctuations of about 100 ms, failing to reach the levels observed in regular exercisers. Regarding the individual depicted in Figure 4c, during the interview, the volunteer disclosed a consistent exercise regimen, with a resting heart rate of approximately 70 bpm in the absence of stimulants. Before measurement, this individual has prior consumed caffeine and did exercise. Analysis of the radar signal on the left indicates a reduction in breathing amplitude, signifying a return to baseline bodily function. Simulation outcomes utilizing the HRV calculation algorithm demonstrate initially diminished HRV levels post-exercise, dropping below 550 ms. Subsequently, HRV rebounds to a higher level exceeding 750 ms. However, due to the caffeine's influence, the cardiac IBI struggles to reach normal levels, resulting in sustained elevated heart rate attributed to sympathetic nervous system activity.

To evaluate the effectiveness of tracking cardiac IBI of three measurement subjects using input stimulation, the Bland-Altman and scatter plot of cardiac IBI evaluation by radar using proposed method and by ECG are shown in Figure 5. Scatter plot shows a correlation of 96.38% between cardiac IBI by proposed method using radar to measure and cardiac IBI by ECG. In the Bland-Altman plot it is shown that there is a close agreement between the cardiac IBI by radar measurement and cardiac IBI by contact-type sensor. The mean bias value of cardiac IBI is 0.39 ms and 95% limits of agreement of cardiac IBI values is 70.37 ms. It can be said that this parameter shows high agreement when the measurement condition of the subjects is right after completing vigorous exercise. In previous research the authors often measured individuals at complete rest, reaching the body's highest static state [35].

Figure 6 illustrates HRV characteristics presented in the frequency domain. The depictions labeled a, b, c correspond to the following profiles in sequence: a) A 33-year-old female, weighing 58 kg, standing at 1.61 m with a resting heart rate of 55-65 bpm; b) A 34-year-old male, weighing 68 kg, standing at 1.69 m with

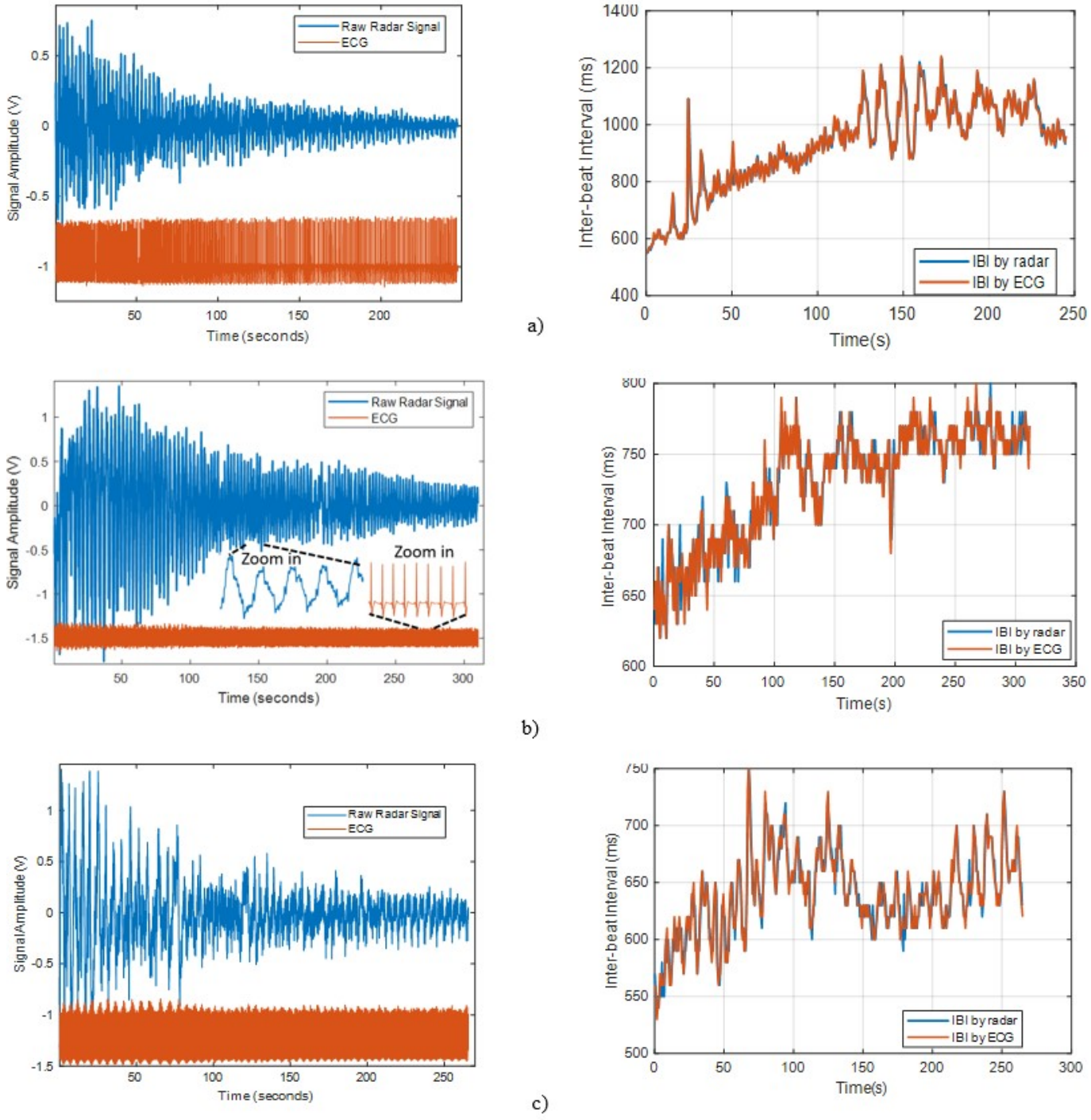


Figure 4. The raw signal measured by radar and ECG of three subjects a) Female, 33 year-old, 58 kg, 1.61 m, HR at rest 55-65 bpm; b) Male 34 year-old, 68 kg, 1.69 m, HR at rest 75-80 bpm; and c) Male 26 year-old, 71 kg, 1.72 m, HR at rest 80-90 bpm.

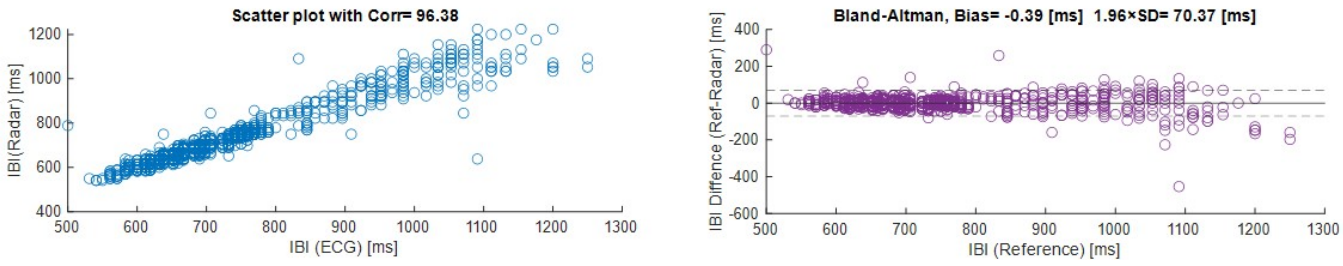


Figure 5. A scatter plot (on the left) and a Bland-Altman plot (on the right) illustrate the results of IBI detection using the proposed method for radar signals and ECG data from three subjects with stimulation input.

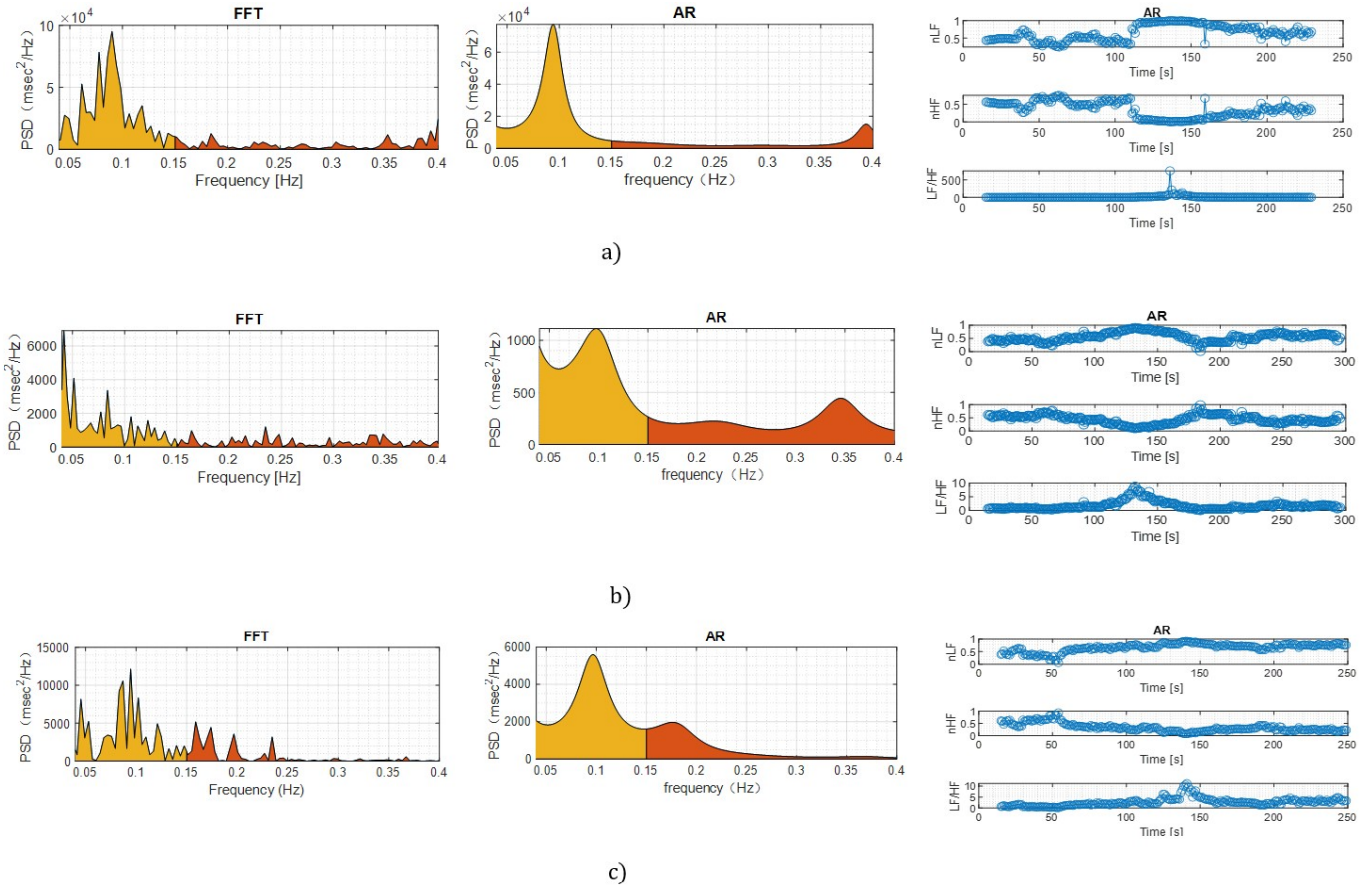


Figure 6. HRV features in the frequency domain. The descriptions in Figures a, b, c are shown in the following order. a) Female, 33 year-old, 58 kg weight, 1.61 m tall, HR at rest of 55-65 bpm; b) Male 34 year-old, 68 kg weight, 1.69 m tall, HR at rest of 75-80 bpm; and c) Male 26 year-old, 71 kg weight, 1.72 m tall, HR at rest of 80-90 bpm.

a resting heart rate of 75-80 bpm; and c) A 26-year-old male, weighing 71 kg, standing at 1.72 m with a resting heart rate of 80-90 bpm. Subjects a and b engaged in exercise before measurement, while subject c exercised and consumed coffee before being measured after 5 minutes. The calculation of cardiac IBI follows the methodology outlined in Figure 3. Subsequently, the cardiac IBI is transformed into the frequency domain using FFT and AR methods as detailed in section 2.3. From Figure 6, the diagram showing power spectral density (PSD), we can observe that the power in the LF region is larger than the power in the HF region, this is explained by the activity of the parasympathetic nerve, when the body is returning to its resting state after completing vigorous exercise. However, the body has not returned to a truly relaxed state. In the figure, the energy of nLF and nHF normalized over time will clearly show the change in power over time. In the period, there is higher nLF power and lower nHF power represent interference from the sympathetic nerves as the body gradually returns to a resting state after doing exercise.

Figures 6a and 6b illustrate the gradual return of the body to a state of recovery, showing distinct breathing frequencies for the volunteers. In Figure 6a, the volunteer exhibits a breathing frequency of approximately 0.4 Hz, whereas in Figure 6b, the frequency is approximately 3.5 Hz. This variance arises from the well-established phenomenon in healthy individuals where breathing induces noticeable fluctuations in heart rate, known as RSA. RSA is a primary aspect of HRV, manifests as the heart rate accelerates during inhalation and decelerates during exhalation. This physiological response occurs due to changes in vagal nerve stimulation and baroreceptor activation in response to alterations in intrathoracic pressure. Notably, HRV is observed solely in subjects who have genuinely recovered. In Figure 6c, the absence of respiratory rate within the high-frequency range, this can surmise that the individual has not truly recovered to a normal state due to the effects of caffeine.

## 5 Discussion and Conclusion

Cardiac IBI and HRV are important information in health diagnosis. From the parameters of HRV, the activity and balance of autonomic nervous function can be inferred. For instance, heart failure is considered a typical condition for disorders and imbalances in autonomic nervous function. The method of extracting cardiac IBI and HRV through the calculation and nonlinear filtering as presented method has resulted in effective evaluation on a group of healthy subjects in a static resting state and also on group of subjects using stimulation that causes increased heart rate. The application of this evaluation on the resting healthy sub-

jects was reviewed and compared to previous studies, confirming the effectiveness of the research approach. The results of evaluating HRV characteristics in the frequency domain in the group of individuals using stimuli that increase heart rate have showed that low frequency power is much higher than high frequency power, this is due to activation of sympathetic nervous system. This observation paves the way for further exploration, utilizing radar technology as a non-contact means to extract vital disease-diagnosing parameters. Regarding the research limitation, firstly, due to the hospital setting where patients typically remain in a supine position, our study focused on measurements conducted in this position, with the radar placed beneath the bed or mattress. To broaden the applicability, it is imperative to explore various measurement positions and postures. Secondly, the dataset comprising healthy subjects is limited in age diversity. Thus, it is crucial to validate the proposed method across a broader age range since different age groups exhibit distinct physiological characteristics, leading to variations in vital signs. Thirdly, the LPNR-based method entails computationally intensive algorithms, posing challenges for real-time implementation. Consequently, achieving real-time computation of HRV remains a targeted objective for the subsequent phase of this study.

## Declarations

All authors declare that they have no confict of interest.

## Acknowledgments

The ASEAN IVO (http://www.nict.go.jp/en/asean_ivo/index.html) project, "Artificial Intelligence Powered Comprehensive Cyber-Security for Smart Healthcare Systems (AIPOSH)", was involved in the production of the contents of this publication and financially supported by NICT (http://www.nict.go.jp/en/index.html).

## References

[1] A. Sapra, A. Malik, and P. Bhandari, "Vital sign assessment," 2020.

[2] S. Erden, N. Demir, G. A. Ugras, U. Arslan, and S. Arslan, "Vital signs: Valid indicators to assess pain in intensive care unit patients? An observational, descriptive study," *Nursing & health sciences*, vol. 20, no. 4, pp. 502–508, 2018.

[3] V. Selvaraju, N. Spicher, J. Wang, N. Ganapathy, J. M. Warnecke, S. Leonhardt, R. Swaminathan, and T. M. Deserno, "Continuous monitoring of vital signs using cameras: A systematic review," *Sensors*, vol. 22, no. 11, p. 4097, 2022.

[4] N. Molinaro, E. Schena, S. Silvestri, F. Bonotti, D. Aguzzi, E. Viola, F. Buccolini, and C. Massaroni, "Contactless vital signs monitoring from videos recorded with digital cameras: an overview," *Frontiers in Physiology*, vol. 13, p. 801709, 2022.

[5] G. Sun, T. Negishi, T. Kirimoto, T. Matsui, and S. Abe, "Noncontact monitoring of vital signs with RGB and infrared camera and its application to screening of potential infection," *Non-invasive diagnostic methods-image processing*, 2018.

[6] M.-Z. Poh, D. J. McDuff, and R. W. Picard, "Advancements in noncontact, multiparameter physiological measurements using a webcam," *IEEE transactions on biomedical engineering*, vol. 58, no. 1, pp. 7–11, 2010.

[7] T. Negishi, S. Abe, T. Matsui, H. Liu, M. Kurosawa, T. Kirimoto, and G. Sun, "Contactless vital signs measurement system using RGB-thermal image sensors and its clinical screening test on patients with seasonal influenza," *Sensors*, vol. 20, no. 8, p. 2171, 2020.

[8] F. Fioranelli, J. Le Kernec, and S. A. Shah, "Radar for health care: Recognizing human activities and monitoring vital signs," *IEEE Potentials*, vol. 38, no. 4, pp. 16–23, 2019.

[9] J.-M. Muñoz-Ferreras, J. Wang, Z. Peng, C. Li, and R. Gómez-García, "FMCW-radar-based vital-sign monitoring of multiple patients," in *Proceedings of the 2019 IEEE MTT-S International Microwave Biomedical Conference (IMBioC)*, vol. 1. IEEE, 2019, pp. 1–3.

[10] G. Paterniani, D. Sgreccia, A. Davoli, G. Guerzoni, P. Di Viesti, A. C. Valenti, M. Vitolo, G. M. Vitetta, and G. Boriani, "Radar-based Monitoring of Vital Signs: A Tutorial Overview. preprint," 2022.

[11] K. Edanami, M. Kurosawa, H. T. Yen, T. Kanazawa, Y. Abe, T. Kirimoto, Y. Yao, T. Matsui, and G. Sun, "Remote sensing of vital signs by medical radar time-series signal using cardiac peak extraction and adaptive peak detection algorithm: Performance validation on healthy adults and application to neonatal monitoring at an NICU," *Computer Methods and Programs in Biomedicine*, vol. 226, p. 107163, 2022.

[12] W. Ren, F. Qi, F. Foroughian, T. Kvelashvili, Q. Liu, O. Kilic, T. Long, and A. E. Fathy, "Vital sign detection in any orientation using a distributed radar network via modified independent component analysis," *IEEE Transactions on Microwave Theory and Techniques*, vol. 69, no. 11, pp. 4774–4790, 2021.

[13] K. Yamamoto, K. Toyoda, and T. Ohtsuki, "Spectrogram-based non-contact RRI estimation by accurate peak detection algorithm," *IEEE Access*, vol. 6, pp. 60 369–60 379, 2018.

[14] V. L. Petrović, M. M. Janković, A. V. Lupšić, V. R. Mihajlović, and J. S. Popović-Božović, "High-accuracy real-time monitoring of heart rate variability using 24 GHz continuous-wave Doppler radar," *IEEE Access*, vol. 7, pp. 74 721–74 733, 2019.

[15] H. T. Yen, M. Kurosawa, T. Kirimoto, Y. Hakozaki, T. Matsui, and G. Sun, "A medical radar system for non-contact vital sign monitoring and clinical performance evaluation in hospitalized older patients," *Biomedical Signal Processing and Control*, vol. 75, p. 103597, 2022.

[16] S. Ahmed, Y. Lee, Y.-H. Lim, S.-H. Cho, H.-K. Park, and S. H. Cho, "Noncontact assessment for fatigue based on heart rate variability using IR-UWB radar," *Scientific Reports*, vol. 12, no. 1, p. 14211, 2022.

[17] Y. Yao, C. Brüser, U. Pietrzyk, S. Leonhardt, S. van Waasen, and M. Schiek, "Model-based verification of a non-linear separation scheme for ballistocardiography," *IEEE journal of biomedical and health informatics*, vol. 18, no. 1, pp. 174–182, 2013.

[18] I. Sadek and J. Biswas, "Nonintrusive heart rate measurement using ballistocardiogram signals: a comparative study," *Signal, Image and Video Processing*, vol. 13, no. 3, pp. 475–482, 2019.

[19] I. Sadek and B. Abdulrazak, "A comparison of three heart rate detection algorithms over ballistocardiogram signals," *Biomedical Signal Processing and Control*, vol. 70, p. 103017, 2021.

[20] M. Pour Ebrahim, F. Heydari, T. Wu, K. Walker, K. Joe, J.-M. Redoute, and M. R. Yuce, "Blood pressure estimation using on-body continuous wave radar and photoplethysmogram in various posture and exercise conditions,"

*Scientific Reports*, vol. 9, no. 1, p. 16346, 2019.
[21] F. Geng, Z. Bai, H. Zhang, Y. Yao, C. Liu, P. Wang, X. Chen, L. Du, X. Li, B. Han *et al.*, "Contactless and continuous blood pressure measurement according to caPTT obtained from millimeter wave radar," *Measurement*, vol. 218, p. 113151, 2023.
[22] F. Shaffer and J. P. Ginsberg, "An overview of heart rate variability metrics and norms," *Frontiers in public health*, vol. 5, p. 290215, 2017.
[23] H. T. Yen, M. Kurosawa, T. Kirimoto, Y. Hakozaki, T. Matsui, and G. Sun, "Non-Contact Estimation of Cardiac Inter-Beat Interval and Heart Rate Variability Using Time-Frequency Domain Analysis for CW Radar," *IEEE Journal of Electromagnetics, RF and Microwaves in Medicine and Biology*, 2023.
[24] K. Li, H. Rüdiger, and T. Ziemssen, "Spectral analysis of heart rate variability: time window matters," *Frontiers in neurology*, vol. 10, p. 426305, 2019.
[25] M. T. La Rovere, G. D. Pinna, R. Maestri, A. Mortara, S. Capomolla, O. Febo, R. Ferrari, M. Franchini, M. Gnemmi, C. Opasich *et al.*, "Short-term heart rate variability strongly predicts sudden cardiac death in chronic heart failure patients," *Circulation*, vol. 107, no. 4, pp. 565–570, 2003.
[26] D. J. Brotman, L. D. Bash, R. Qayyum, D. Crews, E. A. Whitsel, B. C. Astor, and J. Coresh, "Heart rate variability predicts ESRD and CKD-related hospitalization," *Journal of the American Society of Nephrology*, vol. 21, no. 9, pp. 1560–1570, 2010.
[27] H. T. Yen, M. Kurosawa, T. Kirimoto, K. Edanami, and G. Sun, "Proof-of-principle experiment on 24 GHz medical radar for non-contact vital signs measurement," in *Proceedings of the 2021 43rd Annual International Conference of the IEEE Engineering in Medicine & Biology Society (EMBC)*. IEEE, 2021, pp. 6884–6884.
[28] P. Grassberger, R. Hegger, H. Kantz, C. Schaffrath, and T. Schreiber, "On noise reduction methods for chaotic data," *Chaos: An Interdisciplinary Journal of Nonlinear Science*, vol. 3, no. 2, pp. 127–141, 1993.
[29] V. Bisogni, M. F. Pengo, G. Maiolino, and G. P. Rossi, "The sympathetic nervous system and catecholamines metabolism in obstructive sleep apnoea," *Journal of thoracic disease*, vol. 8, no. 2, p. 243, 2016.
[30] X. Han, Q. Zhai, N. Zhang, X. Zhang, L. He, M. Pan, B. Zhang, and T. Liu, "A real-time evaluation algorithm for noncontact heart rate variability monitoring," *Sensors*, vol. 23, no. 15, p. 6681, 2023.
[31] T. Sakamoto, S. Mitani, and T. Sato, "Noncontact monitoring of heartbeat and movements during sleep using a pair of millimeter-wave ultra-wideband radar systems," *IEICE Transactions on Communications*, vol. 104, no. 4, pp. 463–471, 2021.
[32] A. Malliani, M. Pagani, F. Lombardi, and S. Cerutti, "Cardiovascular neural regulation explored in the frequency domain," *Circulation*, vol. 84, no. 2, pp. 482–492, 1991.
[33] V. K. Yeragani, S. Krishnan, H. J. Engels, and R. Gretebeck, "Effects of caffeine on linear and nonlinear measures of heart rate variability before and after exercise," *Depression and anxiety*, vol. 21, no. 3, pp. 130–134, 2005.
[34] B. A. Almeida, A. P. Morales, J. R. C. Ribeiro, Y. G. Ribeiro, F. Sampaio-Jorge, T. Barth, and B. G. Ribeiro, "Impact of Caffeine Intake Strategies on Heart Rate Variability During Post-Exercise Recovery: A Systematic Review and Meta-Analysis." *Current Cardiology Reviews*, 2024.
[35] Y. Rong, A. Dutta, A. Chiriyath, and D. W. Bliss, "Motion-tolerant non-contact heart-rate measurements from radar sensor fusion," *Sensors*, vol. 21, no. 5, p. 1774, 2021.

**Hoang Thi Yen** received B.S degree in Biomedical Electronics Engineering and the M.S. degree in Electronics Engineering from Le Quy Don Technical University, Hanoi, Vietnam, in 2013 and 2019, respectively. Her Ph.D. degree in Biomedical Engineering was received from The University of Electro-Communications (UEC), Tokyo, Japan in 2023. She got IEEE GCCE Excellent Demo Award in 2022 and Best Student Paper Award at ATC Vietnam in 2022. She currently works as a lecturer at Le Quy Don Technical University, Hanoi, Vietnam. Her interests include Biomedical Engineering, Non-contact sensor, Vital signs detection, Machine learning and FPGA-based system design.

**Van-Phuc Hoang** received PhD degree in Electronic Engineering from The University of Electro-Communications, Tokyo, Japan in 2012. He has worked as postdoc researcher, visiting scholar at The University of Electro-Communications, Tokyo, Japan, Telecom Paris, France and University of Strathclyde, Glasgow, UK during the period of 2012-2018. He is working as an Associate Professor, Director with Institute of System Integration, Le Quy Don Technical University, Hanoi, Vietnam. His research interests include digital signal processing, hardware security, VLSI design and intelligent systems for Internet of Things. He was the Technical Program Chair of several IEEE international conferences such as ICDV 2017, MCSoC 2018, SigTelCom 2019, APCCAS 2020 and ATC 2020. He is a member of IEEE.

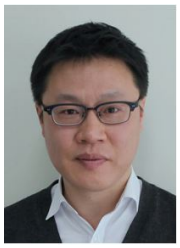

**Guanghao Sun** (Senior Member, IEEE) received the B.S. degree in Medical Engineering from Chiba University, Japan, in 2011. He completed the Frontier Science Course supported by Ministry of Education, Culture, Sports, Science & Technology (MEXT) in Japan, in 2011. His M.S. and Ph.D. degrees in System Design Engineering were received from Tokyo Metropolitan University, Tokyo, Japan, in 2013 and 2015, respectively. From April 2013 to September 2015, he was a Research Fellow of the Japan Society for the Promotion of Science (JSPS). In October 2015, he joined The University of Electro-Communications, Tokyo, Japan, as an Assistant Professor, where he became an Associate Professor in October 2020. His research interests include non-contact bio-measurement, bio-signal processing and design medical instrumentation. He is a Senior Member of IEEE Engineering in Medicine & Biology Society (IEEE-EMBS) and Japanese Society for Medical and Biological Engineering (JSMBE). He received 2013 BESSEC Design Silver Award for design a multiple vital-signs based infection screening system, and 2014 Chinese Government Award for Outstanding Self-financed Student Abroad.